EXCLI Journal 2022;21:722-743 – ISSN 1611-2156
Received: March 09, 2022, accepted: April 13, 2022, published: April 25, 2022

Original article:

CYTOTOXIC CAPABILITY AND THE ASSOCIATED PROTEOMIC PROFILE OF CELL-FREE COELOMIC FLUID EXTRACTS FROM THE EDIBLE SEA CUCUMBER *HOLOTHURIA TUBULOSA* ON HEPG2 LIVER CANCER CELLS

Claudio Luparello[1,*], Rossella Branni[1], Giulia Abruscato[1], Valentina Lazzara[1], Laszlo Drahos[2], Vincenzo Arizza[1], Manuela Mauro[1], Vita Di Stefano[1], Mirella Vazzana[1]

[1] Dipartimento di Scienze e Tecnologie Biologiche, Chimiche e Farmaceutiche (STEBICEF), Università di Palermo, Palermo, Italy
[2] MS Proteomics Research Group, Research Centre for Natural Sciences, Eötvös Loránd Research Network, Budapest, Hungary

* **Corresponding author:** Prof. Claudio Luparello, Dipartimento di Scienze e Tecnologie Biologiche, Chimiche e Farmaceutiche (STEBICEF), Università di Palermo, Edificio 16, Viale delle Scienze, 90128 Palermo, Italy. Tel.: +399123897405; E-mail: claudio.luparello@unipa.it

https://dx.doi.org/10.17179/excli2022-4825

ABSTRACT

Hepatocellular carcinoma (HCC) is an aggressive cancer histotype and one of the most common types of cancer worldwide. The identification of compounds that might intervene to restrain neoplastic cell growth appears imperative due to its elevated overall mortality. The marine environment represents a reservoir rich in bioactive compounds in terms of primary and secondary metabolites produced by aquatic animals, mainly invertebrates. In the present study, we determined whether the water-soluble cell-free extract of the coelomic fluid (CFE) of the edible sea cucumber *Holothuria tubulosa* could play an anti-HCC role *in vitro* by analyzing the viability and locomotory behavior, cell cycle distribution, apoptosis and autophagy modulation, mitochondrial function and cell redox state of HepG2 HCC cells. We showed that CFE causes an early block in the cell cycle at the G_2/M phase, which is coupled to oxidative stress promotion, autophagosome depletion and mitochondrial dysfunction ultimately leading to apoptotic death. We also performed a proteomic analysis of CFE identifying a number of proteins that are seemingly responsible for anti-cancer effects. In conclusion, *H. tubulosa*'s CFE merits further investigation to develop novel promising anti-HCC prevention and/or treatment agents and also beneficial supplements for formulation of functional foods and food packaging material.

Keywords: Hepatocellular carcinoma, invertebrate, echinoderm, cell behavior, protein profile

INTRODUCTION

Hepatocellular carcinoma (HCC) is an aggressive cancer histotype accounting for about 90 % of primary liver tumor cases and is estimated as the sixth most common type of cancer worldwide and the fourth leading cause of cancer-related lethality in the recent years (Suresh et al., 2020; Llovet et al., 2021). Although there are multiple factors involved in the development of HCC, it usually follows

the onset of hepatic cirrhosis from any etiology. Within this context, damaged hepatocytes are addressed to a chronic reparation program based on a high turnover level which ultimately results in the accumulation of genetic alterations and in progressive cell dedifferentiation and modification of the hepatic microenvironment, supporting cell oncogenic transformation (Castelli et al., 2017). HCC prognosis, which often gives rise to extensive metastasis and displays an elevated recurrence rate after resection or ablation, is generally poor and the overall mortality to incidence ratio is estimated to be close to one (McGlynn et al., 2021). The advancement in knowledge of deranged intracellular signalling which leads to HCC development, has prompted the identification of compounds that might intervene on key aspects of the impaired pathways to inhibit neoplastic cell growth (Kumari et al., 2018 and references therein). However, an accurate biological characterization of the molecular mechanism of action of the agents under study is necessary for the development of targeted therapies.

The marine environment, which covers three-quarters of the globe, is rich in extraordinary biodiversity representing a resource of bioindicator organisms and a reservoir of bioactive compounds in terms of primary and secondary metabolites produced by aquatic animals (Chiaramonte et al., 2020; Inguglia et al., 2020; Mauro et al., 2020a; Vazzana et al., 2020a, b). Such molecules regulate very diverse biological activities to implement the necessary adaptation mechanisms for survival in strongly heterogeneous marine ecosystems that are comprised of complex habitats frequently exposed to extreme conditions. These marine-derived natural products have been shown to exert a wide range of therapeutic effects in humans, such as anti-microbial, antioxidant, anti-cancer, anti-inflammatory, wound healing and immunomodulatory effects, thereby interfering with the onset and progress of numerous pathogenic diseases (Senthilkumar and Kim, 2013; Lazzara et al., 2019; Luparello et al., 2020a, b; Luparello, 2021). Based on the health benefits associated with marine bioactives, today's research is also prominently directed to investigate their potential utilization in food and supplement industries (Boziaris, 2014; Suleria et al., 2015; Mauro et al., 2020b; Punginelli, 2021).

Among the marine invertebrate species, Holothurians (i.e. sea cucumbers) have been the object of several studies owing to their curative, nutraceutical and food values which are well-known from traditional folk medicine in several Asian countries (e.g. Correia-da-Silva et al., 2017; Mauro et al., 2021). *Holothuria tubulosa*, an edible sea cucumber species that is widely distributed in the Mediterranean sea including the coasts around Sicily, has been an object of investigations owing to the powerful anti-inflammatory activity of its methanolic extracts, due, at least in part, to the presence of fucoidan, and the anti-microbial activity of peptides contained in its immune cells, the coelomocytes (Herencia et al., 1998; Schillaci et al., 2013; Zhu et al., 2021a). Some research has also previously reported the anti-breast cancer effect of the cell-free aqueous extract of the coelomic fluid (CFE) obtained from this echinoderm (Luparello et al., 2019a). In the present study, we determined whether the CFE of *H. tubulosa* could produce beneficial results against tumors of the digestive apparatus, in particular playing an anti-hepatocarcinoma role, thus representing a novel potential anti-cancer agent deserving further in-depth investigation for functional food purposes. The cell line HepG2, derived from liver biopsies of a 15-year-old Caucasian male with differentiated hepatocellular carcinoma (Donato et al., 2015), was chosen as the model system for this *in vitro* investigation and the effect of the CFE on the viability and locomotory behavior, cell cycle distribution, apoptosis and autophagy modulation, mitochondrial function and cell redox state was tested. Here we report that CFE-treated HepG2 cells are characterized by the inhibition of cell viability, the impairing of cell cycle progress, motile behavior, mitochondrial metabolism, reactive oxygen species (ROS) production, and autophagic flux, and the onset

EXCLI Journal 2022;21:722-743 – ISSN 1611-2156
Received: March 09, 2022, accepted: April 13, 2022, published: April 25, 2022

of apoptotic death. In addition, the data obtained from the proteomic analysis of the CFE identified a number of proteins potentially responsible for the observed impairment of biological activity in HepG2 cells.

MATERIALS AND METHODS

Catching and maintaining of the animals

A sample of 60 healthy adults of *H. tubulosa* sea cucumbers (Figure 1), displaying a length of 11 ± 0.98 cm and a body weight of 46 ± 7.5 g, was fished in the Gulf of Palermo (Sicily, Italy) at a depth of 5–10 m near a grassland of *Posidonia oceanica*. The animals were kept for acclimation in a constantly-aerated aquarium filled with artificial sea water (0.425 M NaCl; 9 mM KCl; 9.3 mM $CaCl_2 \cdot 2H_2O$; 0.0255 M $MgSO_4 \cdot 7H_2O$; 0.023 M $MgCl_2 \cdot 6H_2O$; 2 mM $NaHCO_3$; pH 8.0) at 15 ± 2 °C and fed with commercial invertebrate food (Algamac 3000, Aquafauna Bio-Marine Inc., Hawthorne, CA, USA).

Figure 1: A *Holothuria tubulosa* sea cucumber specimen

Bleeding procedure and preparation of the CFE

The CFE was prepared as described by Luparello et al. (2019a). Briefly, the CF was collected from the animals after making an incision measuring 3–5 cm on the anterior-dorsal side using a scalpel. Samples were held at 4 °C before centrifugation at 1000 g for 10 min at 4 °C to remove coelomocytes. The cell-free CFE was subsequently lyophilized in an Alpha 2–4 LD plus freeze-dryer (Martin Christ, Osterode am Harz, Germany). Aliquots of the samples were resuspended in a minimum volume of sterile distilled water. The CFE protein concentration was evaluated in a Qubit 3.0 fluorometer using the Qubit Protein Assay Kit (ThermoFisher, Waltham, MA, USA) according to the manufacturer's instructions.

Proteomic analysis

The CFE samples were dissolved in 0.25 % RapiGest (Waters Co., Milford, MA, USA) and passed through 10 kDa filters (keeping the retentate) to remove the RIPA buffer, and then the nominal protein concentration was measured for each sample using a NanoDrop 2000 UV-VIS spectrophotometer (ThermoFisher). Ten µg of each sample were reduced using RapiGest and dithiothreitol (ThermoFisher), and subsequently alkylated using iodoacetic acid (ThermoFisher) in 25 mM ammonium bicarbonate buffer (ThermoFisher). Samples were digested in-solution using LysC-trypsin (Mass Spec grade, Promega, Madison, WI, USA) at a 1:100 ratio, then trypsin at a 1:25 ratio. Proteolysis was stopped by adding formic acid (ThermoFisher), and the samples were dried down and cleaned-up using C18 spin columns (Thermo Scientific Sunnyvale, CA, USA) according to the manufacturer's protocol. The cleaned peptide extracts were dried down and stored at -20 °C until analysis.

Aliquots of 1 µg of the tryptic digests were analysed using a Dionex Ultimate 3000 nanoRSLC (Dionex, Sunnyvale, CA, USA) coupled to a Bruker Maxis II ETD mass spectrometer (Bruker Daltonics GmbH, Bremen, Germany) via CaptiveSpray nanobooster ion source. The samples were desalted by 0.1 % trifluoroacetic acid at a flow rate of 5 µL/min for 8 minutes using an Acclaim PepMap100 C-18 trap column (100 µm × 20 mm, Thermo Scientific). The peptides eluting from the pre-column were separated on an ACQUITY UPLC M-Class Peptide BEH C18 column (130 Å, 1.7 µm, 75 µm × 250 mm, Waters) at a 300 nL/min flow rate and 48 °C column temperature using a linear gradient from 4 %

B to 50 % B in 120 minutes. Solvent A was 0.1 % formic acid, and solvent B was acetonitrile with 0.1 % formic acid. The cycle time for data-dependent acquisition, was 2.5 s. MS spectra were acquired at 3 Hz, while MS/MS spectra were acquired at 4 or 16 Hz, depending on the intensity of the precursor ion. Singly charged ions were excluded from the analysis.

The proteins were first identified by searching against the Uniprot Aechinodermata (downloaded: 07/03/2020) database using the Byonic software search engine (v3.8.13, Protein Metrics Inc, San Carlos, CA, USA) with the following parameters: 1 % FDR, 20 ppm peptide mass tolerance, 30 ppm fragment mass tolerance, 2 missed cleavages, trypsin as enzyme, carbamidomethylation of cysteines as fixed modification and following variable modifications (Oxidation/ +15.994915 @ M, Deamidated/+0.984016 @ N, Deamidated/+0.984016 @ Q, Gln->pyro-Glu/-17.026549 @ NTerm Q, Glu->pyro-Glu/ -18.010565 @ NTerm E). Protein hits were filtered by Scaffold (version 4.11, Proteome Software, Inc., USA) using the same parameters stated above in addition to the following parameters: Protein Grouping Strategy: Experiment-wide grouping with protein cluster analysis, Peptide Thresholds: 95.0 % minimum, Protein Thresholds: 1 % FDR and 2 peptides minimum. Subsequently, protein identification was also performed by BlastP comparison to non-redundant protein sequence and model organism databases (available at https://blast.ncbi.nlm.nih.gov/Blast.cgi?PAGE=Proteins; accessed in May 2021). An expected value < 1 was set as cutoff.

Cell culture

The HepG2 HCC cell line was routinely grown in a high glucose–DMEM medium supplemented with 10 % fetal calf serum (Life Technologies, Carlsbad, CA/USA) and antibiotics (100 U/mL penicillin and 100 µg/mL streptomycin; Life Technologies), at 37 °C in a 5 % CO_2 atmosphere.

MTT assay

As an indicator of cytotoxicity, an MTT assay was used to measure cellular activity as reported by Longo et al. (2015). Briefly, exponentially-growing HepG2 cells were seeded in 96-well plates at a concentration of 5500 cells/well and, after overnight adhesion, treatments with different concentrations of CF extract were applied for either 24 or 48 h. After the addition of MTT and cell solubilization, the absorbance of the dissolved formazan was measured in an automated microplate reader at a wavelength of 550 nm. The half maximal inhibitory concentrations (IC_{50}) were evaluated with the Quest Graph IC_{50} calculator (available online: https://www.aatbio.com/tools/ic50-calculator; accessed on 21st June 2021) on the basis of the cell viability ratio between treated and control cells. The subsequent biological assays were performed with CF extracts at the IC_{50} achieved at 24 (IC_{50}24) and 48 h (IC_{50}48), unless otherwise indicated.

Wound healing assay

The scratch/wound healing assay is commonly used to examine the modulation of cell locomotory ability *in vitro* (Luparello et al., 2020a). This experiment was performed as described by Nelson et al. (2014). Briefly, HepG2 cells were seeded in 6-well plates and, once sub-confluent, the monolayer was scraped three times in parallel with a 200 µL pipette tip and a perpendicular line was drawn with a permanent marker. The culture medium was replaced with either plain medium (control) or medium containing CF extracts at IC_{50}24 or at a lesser concentration, i.e. 5 µg/mL, as reported for the evaluation of the wound healing potential of the CF from *Astropecten indicus* sea star on human lung carcinoma cells (Baveja et al., 2018). Selected sites of intersection between the scratched monolayer and the drawn line were photographed under a phase-contrast microscope at time intervals up to 24 h from the start of the assay. Wound healing area measurements were performed on the acquired images using

the ImageJ/Fiji® plug-in developed by Suarez-Arnedo et al. (2020).

Flow cytometry

For each analysis, three independent flow cytometric assays were performed on treated and control cells as previously described (Luparello et al., 2019a, b, 2020c), using a FACSCanto instrument (BD Biosciences, Franklin Lakes, NJ, USA). Ten thousand events were assessed and the obtained data were analyzed with the Floreada analysis tool available at https://floreada.io (accessed in May 2021). Gating in the FSC *vs.* SSC plot was performed to exclude debris, which displayed low FSC values, whereas gating in the FSC-H *vs.* FSC-A plot was performed to exclude doublets and multiplets in cell cycle analyses.

Cell cycle analysis

For the evaluation of cycle phase distribution, cells were fixed with cold 70 % ethanol, treated with 40 μg RNase A/mL, and stained with 20 μg propidium iodide/mL.

Apoptosis analysis

As a hallmark of apoptosis onset, the externalization of phosphatidylserine was evaluated with the Annexin V-FITC kit (Miltenyi Biotec, Bergisch Gladbach, Germany) according to the manufacturer's instructions.

Transmembrane mitochondrial potential (MMP) analysis

The MMP was checked using the JC1 dye (Molecular Probes, Eugene, OR, USA) (Librizzi et al., 2012), which exhibits potential-dependent accumulation in intact mitochondria where the compound undergoes a fluorescence emission shift from green (~529 nm) to red (~590 nm). Thus, in the case of dissipation of MMP, a decrease in the red/green fluorescence intensity ratio can be observed. As a positive control, cells were treated with 1 μM valinomycin, a mitochondria-depolarizing K^+ ionophore.

Reactive oxygen species (ROS) production analysis

The production of ROS was evaluated using the ROS Detection Assay Kit (Canvax Biotech, Cordoba, Spain) which contains the cell-permeant reagent dichlorodihydrofluorescein diacetate (H_2DCFDA), an indicator of reactive oxygen intermediates such as COO- and ONOO-, that becomes fluorescent when oxidized, following the manufacturer's instructions.

Acidic vesicular organelle (AVO) accumulation analysis

Double membrane-AVOs are typically developed by cells undergoing autophagy (Murugan and Amaravadi, 2016; Luparello, 2021). Changes in intracellular AVO accumulation were checked by staining with acridine orange, a green fluorescent dye that, once taken up by acidic vesicles and protonated, forms aggregates that show red fluorescence. For this purpose, flow cytometric analysis was performed on the control and treated cells stained with 100 μg acridine orange/mL (Sigma) for 20 min in the dark after fixation with cold 70 % ethanol.

Statistical analysis

Data were analyzed with analysis of variance (ANOVA) using SigmaPlot 11.0 software (SYSTAT, San Jose, CA, USA). A p-value < 0.05 was considered statistically significant.

RESULTS

CFE inhibits HepG2 cell viability and affects cell cycle progress

In the first set of experiments, we checked the effect of dose- and time-dependent incubation with the aqueous CFE from *H. tubulosa* on HepG2 cell viability *via* an MTT assay. As shown in Figure 2, the number of CFE-treated viable cells decreased in a protein concentration-dependent manner both after 24 and 48 h exposures with an average IC_{50}24 and IC_{50}48 of 20.75 and 16.5 μg/mL, respectively. Once the cytotoxic potential of the preparation was confirmed, all subsequent

EXCLI Journal 2022;21:722-743 – ISSN 1611-2156
Received: March 09, 2022, accepted: April 13, 2022, published: April 25, 2022

assays aimed to reveal more detailed data on the biological mechanism of CFE-induced perturbations were carried out by exposing HepG2 cells at the $IC_{50}24$ and $IC_{50}48$ of the CFE.

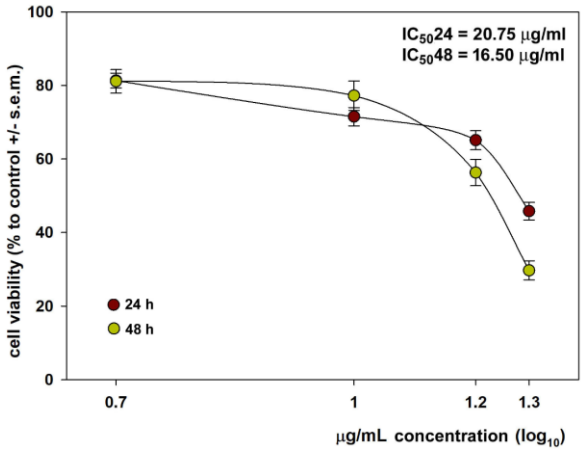

Figure 2: Dose-response effect of CFE from *H. tubulosa* at 2.5, 5, 10 and 15 µg/ml concentration on the viability of HepG2 cells after either 24 (brown circles) or 48 h (green circles) of exposure. Error bars correspond to the standard error of the mean (s.e.m.) of three independent measurements. *P* values comparing viability ratios to controls were < 0.05 for every measurement.

Then, CFE-exposed HepG2 cells were tested for the distribution of the cell population in the cell cycle phases. As shown in Figure 3, 24 h of exposure to the $IC_{50}24$ decreased the percentage of G_0/G_1 and S phase cells (control *vs.* treated = 46.08 % *vs.* 18.35 % and 17.2 *vs.* 8.85 %, respectively) and increased the sub-G_0 population (control *vs.* treated = 10.06 % *vs.* 48.61 %) suggesting a restrained progression into a new cell cycle after mitosis required to activate repair mechanisms or apoptosis and an accumulation of cells with less bright or fragmented DNA, i.e. necrotic or apoptotic. The additional impairment of the G_2/M phase fraction observed after 48 h of treatment with the $IC_{50}48$ of the CFE (control *vs.* treated = 30.98 % *vs.* 17.33 %), the further decrease of the percentage of G_0/G_1 and S phase cells (control *vs.* treated = 48.79 % *vs.* 12.67 % and 13.37 % *vs.* 4.65 %, respectively) and the increase in the percentage of cells in the sub-G_0 fraction (control *vs.* treated = 6.72 % *vs.* 66.13 %) was indicative of prominent cell cycle arrest and cell death as a result of prolonged exposure.

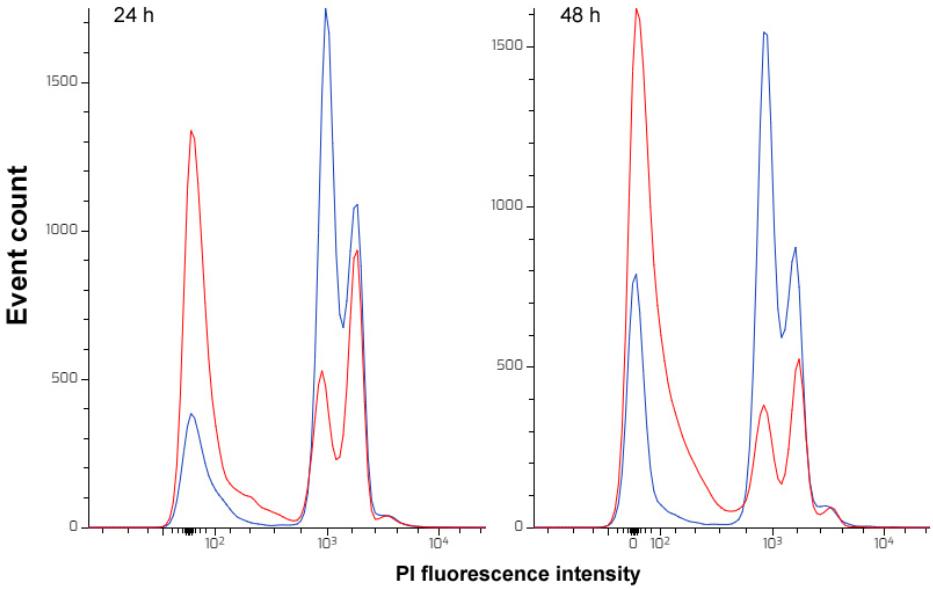

	control	treated
subG0	10.06 +/- 1.1%	48.61 +/- 1.86%
G0/G1	46.08 +/- 3.16%	18.35 +/- 1.07%
S	17.2 +/- 1.47%	8.85 +/- 0.13%
G2/M	25.88 +/- 3.36%	23.54 +/- 0.71%

	control	treated
subG0	6.72 +/- 0.13%	66.13 +/- 0.38%
G0/G1	48.79 +/- 1.59%	12.67 +/- 0.93%
S	13.37 +/- 3.25%	4.65 +/- 0.19%
G2/M	30.98 +/- 1.71%	17.33 +/- 0.59%

Figure 3: DNA profiles of control (blue line) and CFE-treated (red line) HepG2 cells after 24 and 48 h of exposure to the $IC_{50}24$ and $IC_{50}48$ of the preparation, respectively. Cell cycle distribution is reported in the annexed tables for both cell samples (mean ± s.e.m. of three independent experiments).

EXCLI Journal 2022;21:722-743 – ISSN 1611-2156
Received: March 09, 2022, accepted: April 13, 2022, published: April 25, 2022

CFE increases the percentage of apoptotic HepG2cells

To determine whether the observed impairment of cell cycle progress could be at least in part ascribed to an apoptosis-promoting effect of the CFE on HepG2 cells, exposed and control samples were assayed for the externalization of phosphatidylserine using recombinant annexin-V conjugated to green fluorescent FITC dye in conjunction with propidium iodide (PI) as an indicator of cell viability. As shown in Figure 4, the flow cytometric data indicated that after 24 h of exposure to the IC_{50}24 of the CFE the proportion of viable cells decreased from about 83 % of the controls to about 48 %. In contrast, the percentage of late apoptotic cells (annexin-V^+/PI^+) increased from about 14 % of the controls to about 34 %, whereas that of early apoptotic cells (annexin-V^+/PI^-) increased from about 1 % of the control to about 16 %. This result is in line with the previous data regarding the amount of the sub-G_0 cell population after 24 h of exposure to the CFE. No significant difference was found between the control and annexin-V^-/PI^+ cells, commonly regarded as the necrotic population.

CFE provokes the dissipation of MMP and the initial up-regulation of ROS in HepG2 cells

Extensive damage to the mitochondria may lead cells to apoptotic death (Ly et al., 2003). However, a strong positive correlation was observed between the MMP and the production of ROS which are known to act as signaling molecules in a plethora of intracellular pathways regulating both cell survival/proliferation and cell death (Zhang et al., 2016; Gao et al., 2020). To detect variation of MMP in CFE-exposed HepG2 cells we used the mitochondria-selective JC1 probe and evaluated the quantity of cells with bright green/bright red emission (endowed with intact MMP) and those with bright green/dim red emission (affected by MMP collapse) in control and treated preparations. CFE caused the dissipation of MMP. In particular, as shown in Figure 5, the percentage of dim red-emitting cells increased from about 27 and 25 % of the controls to about 58 and 98 % in cells incubated with IC_{50}24 CFE for 24 h and IC_{50}48 CFE for 48 h, respectively. In the latter case, this proportion was very similar to that of the valinomycin-exposed positive control.

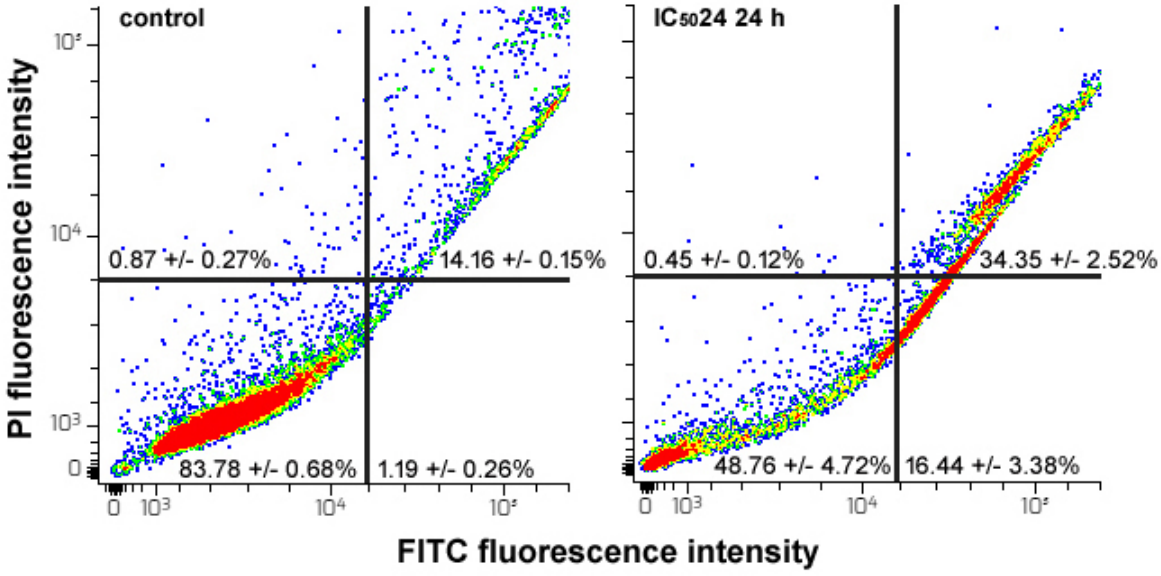

Figure 4: Flow cytometric assays for apoptosis in HepG2 cells cultured in control conditions or exposed to CFE IC_{50}24 for 24 h. The plots show the results of representative experiments and the percentages, indicated as the mean ± s.e.m. of three independent experiments, refer to viable annexin-V^-/PI^- cells (bottom left quadrant), early apoptotic annexin-V^+/PI^- cells (bottom right quadrant), late apoptotic annexin-V^+/PI^+ cells (top right quadrant) and necrotic annexin-V^-/PI^+ cells (top left quadrant).

EXCLI Journal 2022;21:722-743 – ISSN 1611-2156
Received: March 09, 2022, accepted: April 13, 2022, published: April 25, 2022

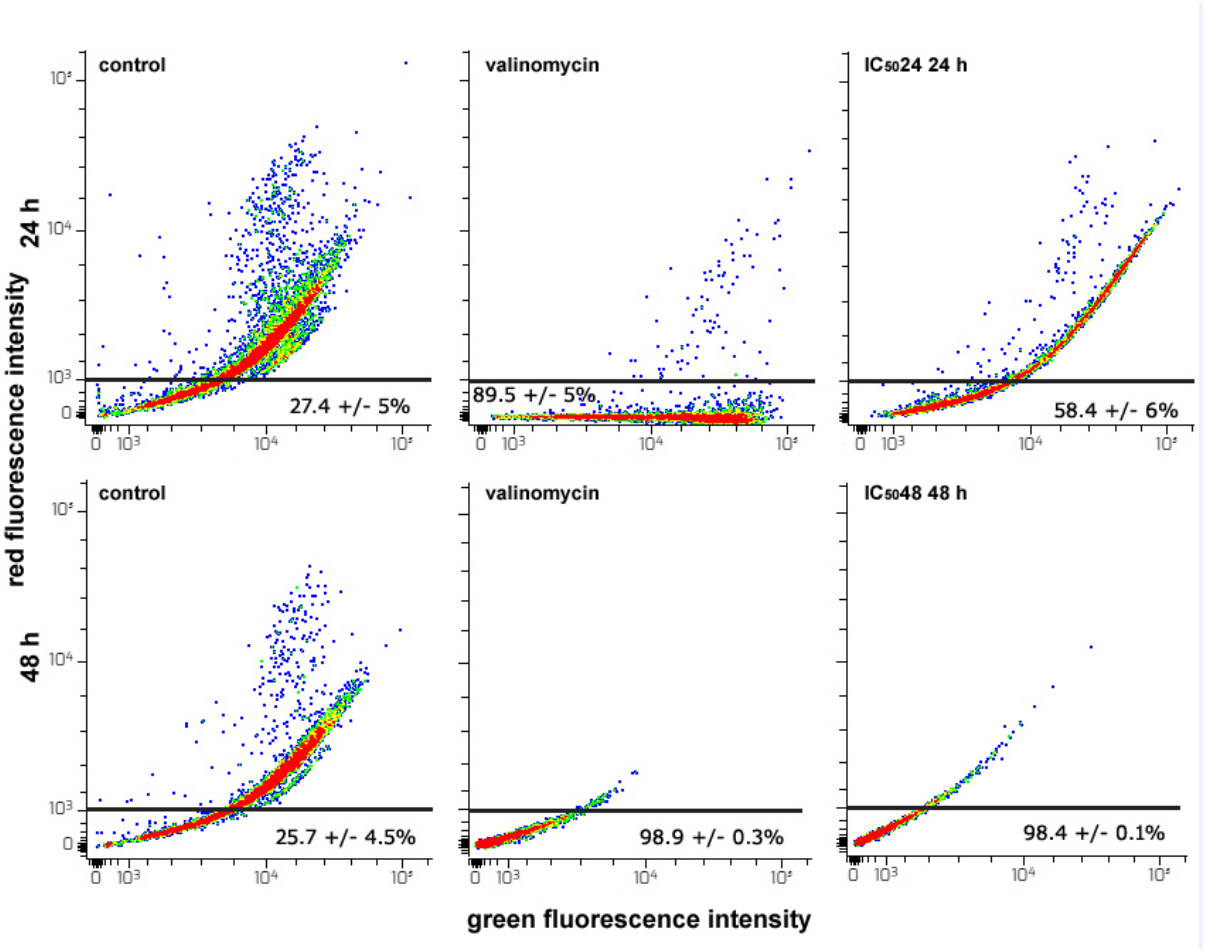

Figure 5: Flow cytometric assays for MMP in HepG2 cells cultured for 24 or 48 h in control conditions, in the presence of 1 µM valinomycin, and of either CFE IC_{50}24 or CFE IC_{50}48. The plots show the results of representative experiments and the percentages in the bottom quadrants of each frame, indicated as the mean ± s.e.m. of three independent experiments, are referred to dim red-emitting cells that underwent MMP dissipation.

The ability of the CFE to affect mitochondrial metabolism was also determined by evaluating the accumulation of ROS. To detect variation in ROS production in CFE-exposed HepG2 cells we used the H_2DCFDA probe and evaluated its oxidation to green-emitting DCF by various peroxide-like and nitric oxide-derived reactive molecules. In each sample, the flow cytometric data revealed the presence of two distinct cell subpopulations endowed with low (ROS^-) and high rates (ROS^+) of ROS generation. The mean fluorescence intensity (MFI) values of the events associated with the ROS^+ subpopulations were recorded to compare their rates in the different experimental conditions. In addition, the percentage of ROS^+ cells within the whole populations was calculated. Taking the data reported in Figure 6A and B into account, a transient up-regulation in ROS generation could be observed after 24 h incubation with the CFE with a 1.45-fold-ROS increase in exposed *vs.* control cells (control cells' MFI = 6727, treated cells' MFI = 9770; $P< 0.05$). On the other hand, the ROS^+ cell amount was smaller than that of controls (about 18 %) after 24 h of treatment with IC_{50}24 CFE. This may suggest the initial occurrence of an increased intracellular ROS production coupled with an extended cell damage, both aspects that fit well with the already-reported significant decrease of MMP with consequent deterioration of cells' respir-

EXCLI Journal 2022;21:722-743 – ISSN 1611-2156
Received: March 09, 2022, accepted: April 13, 2022, published: April 25, 2022

atory activity. As expected from the progressive advancement of cellular impairment and death, HepG2 cells exposed to IC_{50}48 CFE for 48 h showed a drastic arrest of ROS overproduction *vs.* control cells (control cells' MFI = 1166; treated cells' MFI = 960; no statistical significance).

CFE impairs HepG2 cell autophagic behavior

To determine whether the CFE could modify the autophagic behavior of HepG2 cells, acridine orange staining was performed to label AVOs, a hallmark of autophagic cells. In fact, as reported by Gibson (2013), flow cytometric scanning of changes in the amount of AVOs is indicative of variations in autophagosome accumulation and autolysosome formation. Analysis of the plots revealed the constant presence of two distinct cell subpopulations characterized by low (AVO^-) and high rate (AVO^+) of acridine orange fluorescence. Consistent with the data from Sun et al. (2018), these results confirmed that HepG2 cells are endowed with a high basal level of autophagy, with the percentage of AVO^+ actively-autophagic cells being about 69 and 74 % at 24 and 48 h of culture, respectively, under control conditions (Figure 7A, C). However, the proportion of AVO^+ cells decreased 24 h after treatment with IC_{50}24 CFE (25 %; Figure 7B). Further incubation for 48 h with the IC_{50}48 indicated the almost complete disappearance of the AVO^+ cell population, whose proportion dropped to about 2 % (Figure 7D).

CFE inhibits HepG2 cell migration in vitro

Wound healing assays were performed and monitored within 24 h to examine the effect of incubation with the aqueous CFE from *H. tubulosa* on HepG2 cell locomotory ability. As illustrated by Figure 8, under control conditions, HepG2 cell migration determined the advancing reduction of the denuded area (mean area % = 23 at time 0), which had already started at 2 h from the scratch time (mean area % = 17) leading to partial obliteration after 6 h (mean area % = 6) and then total closure of the wound within 24 h. In contrast, exposure to IC_{50}24 CFE inhibited cells' ability to migrate into the scratch area, and, as expected, cells in the last period of treatment displayed signs of suffering and damage such as rounding and detaching from the substrate. Based on the data by Baveja et al. (2018) who demonstrated a non-cytotoxic and effective wound healing–effect of 24 h-administration of 5 µg/mL of the CFE from another invertebrate species, the sea star *A. indicus*, to human A-549 tumor cells, we also tested HepG2 cells' migratory behavior in the presence of *H. tubulosa*'s CFE at low concentration. As revealed in the panel, although the cells' healthy morphological appearance appeared unmodified by the treatment, a slight sign of

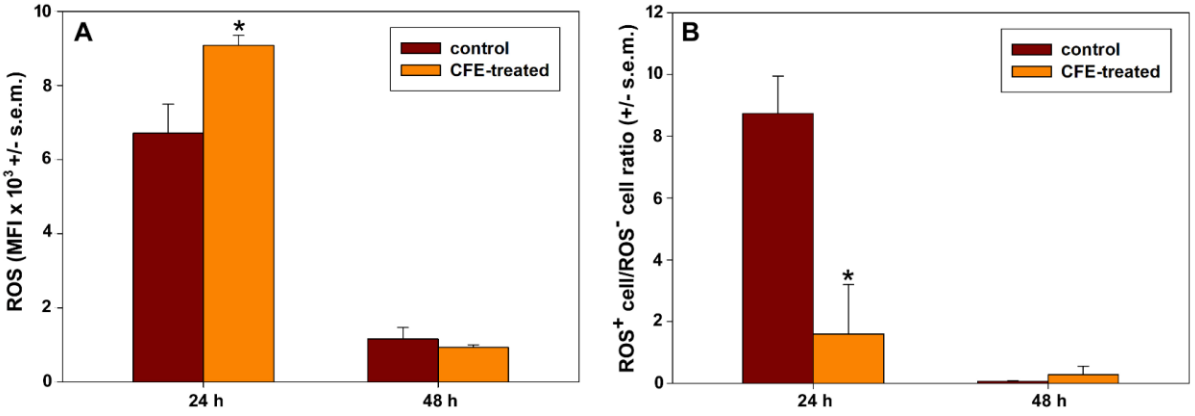

Figure 6: Bar graphs showing the ROS-associated MFI in ROS^+ cell subpopulations (**A**) and the ROS^+ cell/ROS^- cell ratio (**B**) in parallel preparations of control and IC_{50}24 and IC_{50}48 CFE-treated HepG2 cells for 24 and 48 h (mean ± s.e.m. of three independent experiments). * $p < 0.001$ (**A**) and = 0.029 (**B**) determined with independent t-tests.

EXCLI Journal 2022;21:722-743 – ISSN 1611-2156
Received: March 09, 2022, accepted: April 13, 2022, published: April 25, 2022

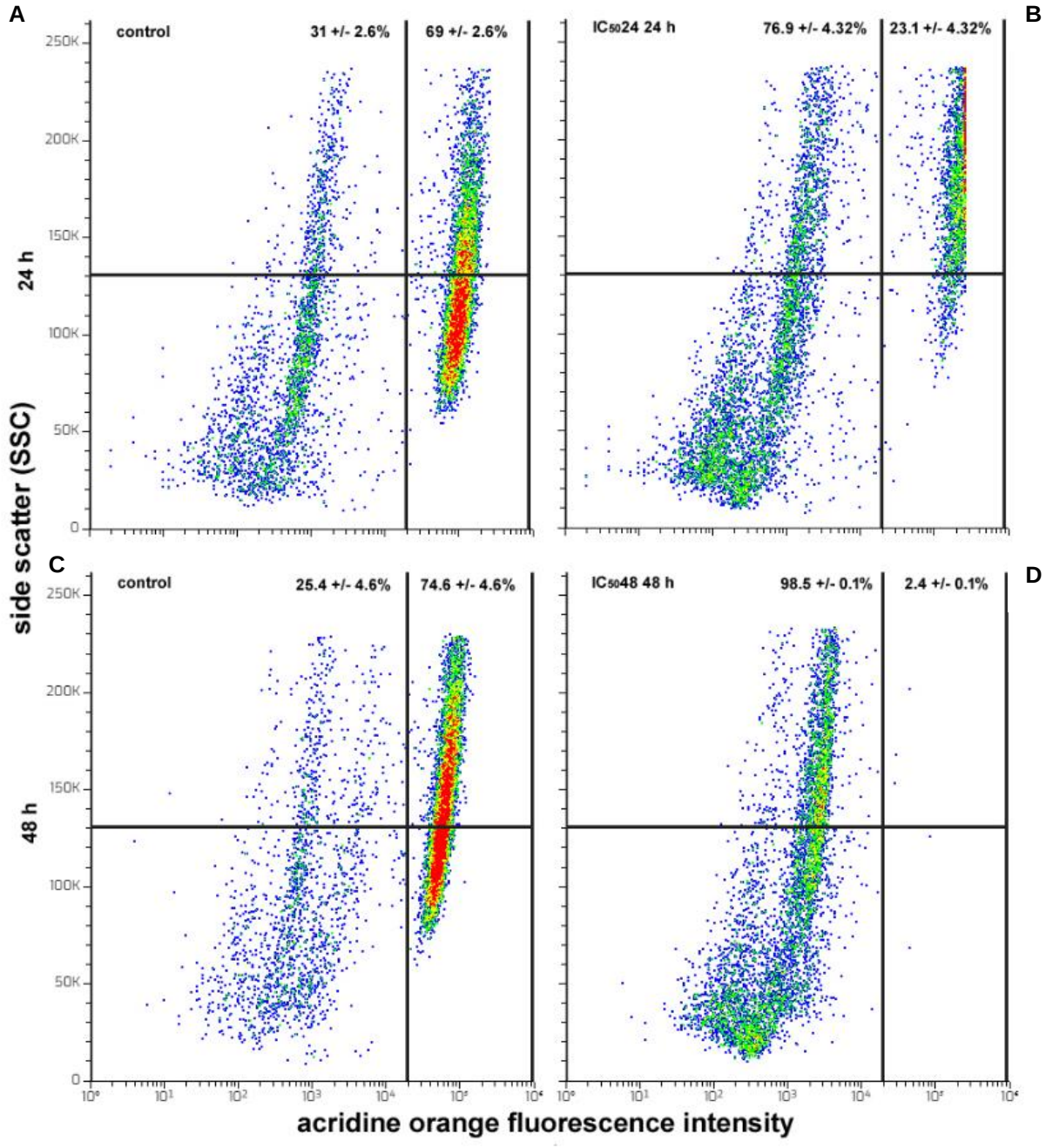

Figure 7: Flow cytometric assays for AVOs in HepG2 cells cultured in control conditions for 24 (**A**) and 48 h (**C**) or exposed to CFE IC_{50}24 for 24 h (**B**) and CFE IC_{50}48 for 48 h (**D**). The plots show the results of representative experiments and the percentages, indicated as the mean ± s.e.m. of three independent experiments, refer to AVO^+ cells (right quadrants) and AVO^- cells (left quadrants).

reduction in the scratch area was observed only at 24 h after exposure (mean area % at time 0 and after 24 h = 24 and 19, respectively), thereby confirming the migration-inhibiting effect exerted by *H. tubulosa*'s CFE on liver cancer cells.

Proteomic profile of the CFE identifies potential contributors to the observed cytotoxic activity

It is widely acknowledged that peptides and proteins produced by marine invertebrates may be endowed with cell death-promoting properties, such as the ability to induce

EXCLI Journal 2022;21:722-743 – ISSN 1611-2156
Received: March 09, 2022, accepted: April 13, 2022, published: April 25, 2022

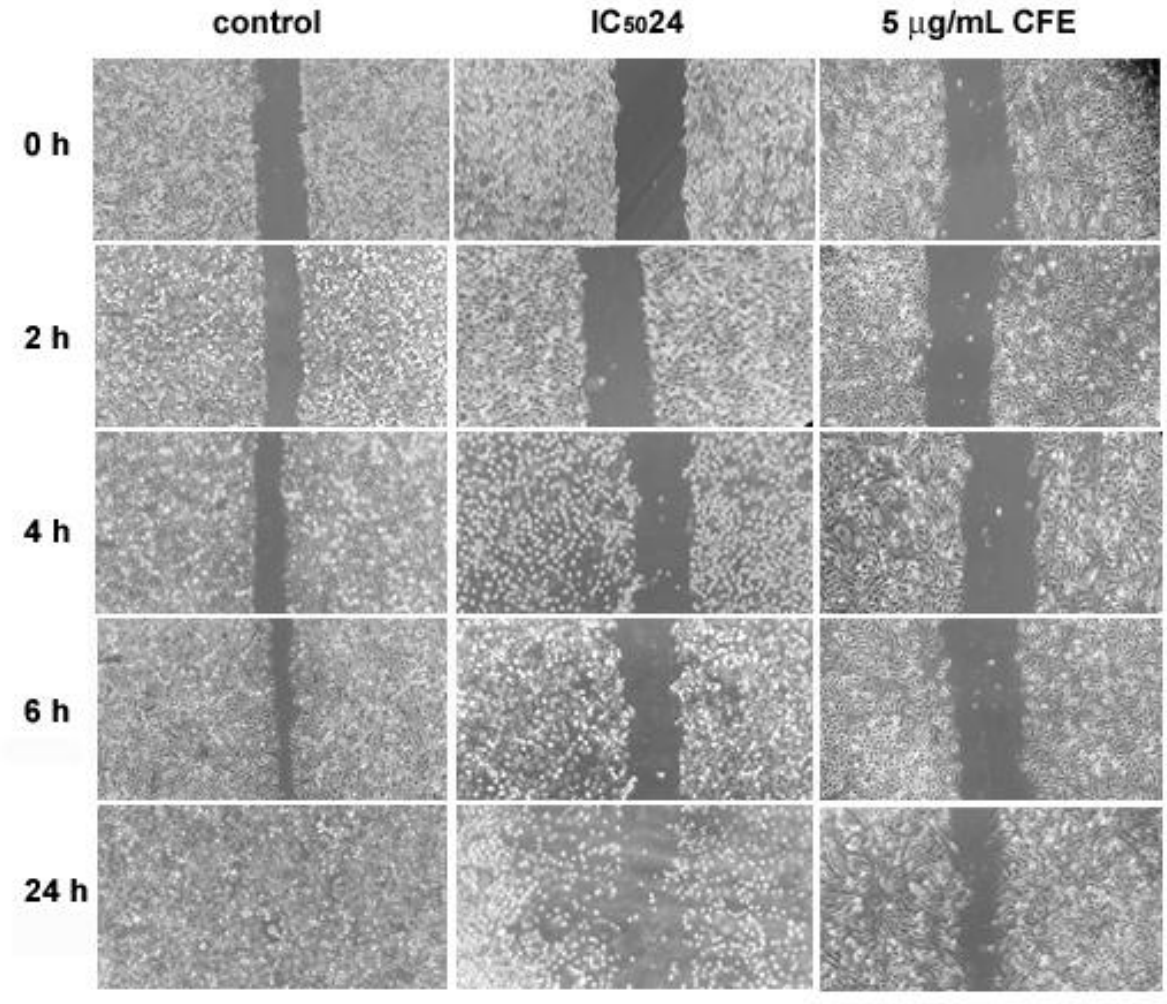

Figure 8: Representative phase-contrast micrographs acquired during wound-healing experiments at different time intervals under control conditions, and in the presence of CFE at $IC_{50}24$ and 5 µg/mL concentration. The assay was performed in triplicate. Microscopic magnification = 20X

apoptosis, activate the mitochondrial intrinsic pathway and/or impair signal transduction pathways as well as cytoskeletal dynamics (Zheng et al., 2011). Based on the observed cytotoxic role played by the CFE from *H. tubulosa* on HepG2 tumor cells, proteomic analysis of the aqueous preparations was performed after proteolysis of the samples and MS sequencing to detect bioactive components. Overall, 1648 obtained spectra matched forward peptides and the final output reported 115 forward and 20 reverse proteins and 321 unique forward peptides. The estimated spectrum-level FDR on true proteins was 0.1 %. A bioinformatic similarity search against the different databases identified 18 proteins contained in the CFE that are potentially associated with the various aspects related to the impairment of HepG2 cell biological activities reported in the previous paragraphs, as well as with exosome secretion. The peptide sequences and the results of alignments selected on the basis of sorting by the best E value are reported in Table 1.

EXCLI Journal 2022;21:722-743 – ISSN 1611-2156
Received: March 09, 2022, accepted: April 13, 2022, published: April 25, 2022

Table 1: Cytotoxic activity-associated protein profile of the CFE from *H. tubulosa*

Peptide sequence(s)	Sequence ID (no. of matches/range)	Expected	Identities (%)	Positives (%)	Protein description	Organism	Selected protein categories
LVGGTFAQ[+0.984]EGR	PIK44174.1 (2/275-287, 382-394)	0.003/0.003	100/100	100/100	Putative Deleted In Malignant Brain Tumors 1 (DMBT1) protein-like	*Stichopus japonicus* (sea cucumber)	
LVGGNTDSEGR	PIK52969.1 (1/358-370)	0.005	100	100	Putative DMBT1 protein isoform X4-like		
LVGGSNSSEGRV	XP_030851619.1 (1/1663-1675)	0.013	100	100	DMBT1 protein-like	*Strongylocentrotus purpuratus* (sea urchin)	-membrane -scavenger receptor activity -endocytosis
LVGGSNSTEGR	XP_011666462.2 (1/736-748)	0.009	100	100/92	DMBT1 protein-like		
LVGGSNSAEGR	XP_030851596.1 (2/973-985, 1187-1199)	0.013/0.1	100/92	100	DMBT1 protein-like		
LVDGASPNEGR	XP_030839388.1 (1/112-124)	0.003	100	100	DMBT1 protein-like		
LVGGSNALEGR	XP_030857505.1 (1/1509-1601)	0.009	100	100	DMBT1 protein		
LVGGASNAEGR	XP_030851622.1 (1/1071-1083)	0.013	100	100	DMBT1 protein-like		
LVGGSSDNEGR	XP_030833786.1 (5/857-869, 1084-1096, 1311-1323, 1538-1550, 1765-1777)	0.006/0.006/0.006/0.1/0.1	100/100/100/92/92	100/100/100/92/92	DMBT1protein isoform X1 (also X2-X4)		
LANGSTANEGR	XP_030832692.1 (1/696-708)	0.006	100	100	DMBT1protein isoform X1 (also X2-X4)		
LVGGSSDSEGR	XP_041455825.1 (2/241-252, 1906-1917)	0.15/0.15	100/100	100/100	DMBT1 protein-like	*Lytechinus variegatus* (sea urchin)	

EXCLI Journal 2022;21:722-743 – ISSN 1611-2156
Received: March 09, 2022, accepted: April 13, 2022, published: April 25, 2022

Table 1 (cont.): Cytotoxic activity-associated protein profile of the CFE from *H. tubulosa*

Peptide sequence(s)	Sequence ID (no. of matches/range)	Expected	Identities (%)	Positives (%)	Protein description	Organism	Selected protein categories
LSYLTNQADYELR	PIK57223.1 (1/111-125)	$3e^{-06}$	100	100	Putative ficolin 2-like	*Stichopus japonicus* (sea cucumber)	-extracellular exosome -signaling receptor binding -immune defense process
RIDGSIDFSR	PIK56797.1 (1/60-71)	0.006	100	100	Putative ficolin 2-like		
IAFLTNQKQYQLR	PIK37772.1 (1/21-34)	$2e^{-04}$	93	100	Putative ficolin 2-like		
NGFGFLGSEFWIGNEK	PIK59961.1 (1/94-111)	$8e^{-10}$	100	100	Ficolin 2		
NGFGELDHEFWLGNDK	PIK55963.1 (1/213-230)	$5e^{-10}$	100	100	Putative ficolin 2		
ETAVEAVNQGK	PIK52263.1 (1/83-95)	0.001	100	100	Putative semaphorin-1A	*Stichopus japonicus* (sea cucumber)	- semaphorin receptor binding
TVN[+0.984]TFAFK	PIK33946.1 (1/227-236)	0.33	100	100	Putative beta-1,3-glucan-binding protein	*Stichopus japonicus* (sea cucumber)	-extracellular region -pattern recognition receptor activity -immune system process
GDWIWPAIWLLPK	PIK33946.1 (1/247-261)	$4e^{-8}$	100	100			
QVLTQAEGLVR	PIK61193.1 (1/430-442)	0.002	100	100	Putative TBC1 domain family ‘member 17	*Stichopus japonicus* (sea cucumber)	-intracellular protein transport -activation of GTPase activity -autophagy
RSAPSQGPNNG	PIK47307.1 (1/459-471)	0.005	100	100	Putative huntingtin-interacting protein 1 isoform X3	*Stichopus japonicus* (sea cucumber)	-actin filament binding -endocytosis -apoptotic process
RIEELTELL	XP_030854451.1 (1/312-322)	0.05	100	100	Apoptosis-stimulating of p53 protein 1 isoform X1	*Strongylocentrotus purpuratus* (sea urchin)	-p53 binding -negative regulation of cell cycle -regulation of apoptotic process

Table 1 (cont.): Cytotoxic activity-associated protein profile of the CFE from *H. tubulosa*

Peptide sequence(s)	Sequence ID (no. of matches/range)	Expected	Identities (%)	Positives (%)	Protein description	Organism	Selected protein categories
LSQGTINPTTR	XP_030844441.1 (1/479-491)	0.002	100	100	Zinc finger C3H1 domain-containing protein isoform X3	*Strongylocentrotus purpuratus* (sea urchin)	-nucleus -RNA processing -protein binding
QYNEIISR	PIK43820.1 (1/212-221)	0.16	100	100	Putative endoplasmic reticulum resident protein 44	*Stichopus japonicus* (sea cucumber)	-extracellular exosome -protein binding - response to unfolded protein
RGDVDFTNLI	XP_030837943.1 (1/392-403)	0.008	100	100	Galactosylceramide sulfotransferase	*Strongylocentrotus purpuratus* (sea urchin)	-membrane -sphingolipid metabolic process -transferase activity
INFER LYEGCIDDAK	XP_030854500.1 (1/560-566) XP_030854500.1 (1/575-586)	$1e^{-8}$ $1e^{-8}$	100 100	100 100	Pre-mRNA-processing factor 39	*Strongylocentrotus purpuratus* (sea urchin)	-nucleus -protein binding -mRNA processing
LWAYVTIK	PIK55236.1 (1/78-87)	0.12	100	100	Putative inter-alpha-trypsin inhibitor heavy chain H3	*Stichopus japonicus* (sea cucumber)	-extracellular exosome -serine-type endopeptidase inhibitor activity
FYEYIMEYK	AAR89380.1 (1/79-89)	$7e^{-7}$	100	100	Ependymin-related protein precursor	*Holothuria glaberrima*	-lysosome -extracellular region -protein binding

Table 1 (cont.): Cytotoxic activity-associated protein profile of the CFE from *H. tubulosa*

Peptide sequence(s)	Sequence ID (no. of matches/range)	Expected	Identities (%)	Positives (%)	Protein description	Organism	Selected protein categories
RSSTPIYSI	XP_030855587.1 (1/2485-2495)	0.14	100	100	Nesprin-1 isoform X1	*Strongylocentrotus purpuratus* (sea urchin)	-cytoskeleton -integral component of the membrane -actin filament-binding
	XP_030855588.1 (1/2479-2489)	0.14	100	100	Nesprin-1 isoform X2		
	XP_030855589.1 (1/2478-2488)	0.14	100	100	Nesprin-1 isoform X3		
	XP_030855590.1 (1/2468-2478)	0.14	100	100	Nesprin-1 isoform X4		
AGLQFPVGR	XP_030843320.1 (1/21-31)	$6e^{-05}$	100	100	Histone H2A-like	*Strongylocentrotus purpuratus* (sea urchin)	
GTGASGTFK	PIK36764.1 (1/77-87)	0.001	100	100	Histone H1-beta	*Stichopus japonicus* (sea cucumber)	
GTGASGSFK	XP_033108982.1 (1/78-87)	0.023	100	100	Late histone H1-like	*Anneissia japonica* (sea lily)	
ESYSIYIYK	P48557.1 (1/32-42)	$1e^{-5}$	100	100	Histone H2B	*Holothuria tubulosa*	
AMSIMNSFVNDIFER	P48557.1 (1/55-71)	$2e^{-12}$	100	100			
EVQTAVR	XP_030836142.1 (1/89-97)	0.003	100	100	Histone H2B	*Strongylocentrotus purpuratus* (sea urchin)	
LLLPGELAK	XP_030836142.1 (1/96-106)	$3e^{-05}$	100	100			

EXCLI Journal 2022;21:722-743 – ISSN 1611-2156
Received: March 09, 2022, accepted: April 13, 2022, published: April 25, 2022

DISCUSSION

Holothurians are known to be exploited for human food purposes and as a remedy in traditional medicine, and in the present paper we determined whether the water-soluble CFE from *H. tubulosa* could exert any cytotoxic effect against an *in vitro* cell model of a cancer of the digestive system, i.e. hepatocellular carcinoma. Our data depicted an anti-tumoral role of the preparation, at least under the conditions used, characterized by an early block of the cell cycle at the G_2/M phase coupled to oxidative stress promotion, AVO depletion and mitochondrial dysfunction and leading to apoptotic death.

G_2/M arrest is an event commonly preceding apoptosis (Chen et al., 2021; Tawfik et al., 2021) which, as reviewed by DiPaola (2002), may be based upon G_2 checkpoint impairment or problems in the assembly and dynamics of mitotic spindle structure, an aspect that requires further investigation. Elevated levels of basal autophagy in cancer cells, such as HepG2, are instrumental for enabling their survival and active growth and locomotion by fulfilling the high metabolic and energetic demands (Luparello, 2021). Thus, a possible mechanism of CFE cytotoxicity may involve the suppression of "protective" autophagy which, as reported by Zhu et al. (2021b) for chitooligosaccharide-treated HepG2 cells, leads to the inhibition of cell proliferation and apoptosis *via* the intrinsic pathway as suggested in our model system by the collapse of MMT. Mitochondria are both primary sources and targets of ROS (Marchi et al., 2012). However, HepG2 cells express low levels of cytochrome P450 family 2 subfamily E member 1 (CYP2E1), a ROS-generating enzyme of the endoplasmic reticulum, and therefore are a useful model to check the formation of ROS mainly from mitochondrial sources (Jiang et al., 2015). Thus, CFE-triggered respiratory deficiency might affect mitochondrial ATP synthesis, and the impairment of the respiratory chain and the oxidative phosphorylation system could stimulate the leakage of electrons from the transport chain with consequent up-regulation of ROS production. In turn, this could establish a vicious cycle of an oxidative stress-induced increase of mitochondrial damage, also at the transcriptome level, with consequent further ROS production. Additionally, impairment of the autophagic flux, which is a common mechanism for the clearance of damaged ROS-overproducing mitochondria, may participate in this vicious cycle and contribute to cell death triggering (Kongara and Karantza, 2012). The derangement of HepG2 cells' healthy state appeared also responsible for an early block of cell locomotory behavior, even at a CFE dose less than the IC_{50}24, thereby suggesting that the preparation may be a potential suppressor of HCC metastatic attitude, even at low concentrations.

The biochemical compositions of extracts from the isolated tegument and dried body of *H. tubulosa* have been the object of some publications that have also provided evidence of the anticancer and antioxidant potential of the preparations (Alper and Güneş, 2020; Zmemlia et al., 2020). To the best of our knowledge, no study is available in the literature on the biochemical composition of the coelomic fluid of *H. tubulosa*, which represents a significant portion of its mass and contains a complex mixture of soluble molecules secreted constitutively by different parts of the invertebrate's body. Therefore, in search of molecular constituents that may conceivably be involved in the observed cytotoxic activity, we complemented cellular assays with a first-released proteomic analysis of the CFE. This study predicted a number of putative anticancer proteins responsible for the lethal effect against HepG2 cells. In parallel, exosome-linked signatures were also detected suggesting the release of extracellular vesicles carrying, among the others, the intracellular constituents likely causing the anti-HepG2 effects in the coelomic fluid of *H. tubulosa*. Exosomes are conceivably preserved intact by the method of preparation of the CFE and therefore could be ready to fuse with and transfer their cargo into cancer cells. Notably, the presence of exosomes in the coelomic fluid of aquatic invertebrates has been

acknowledged and related to their involvement in cell-to-cell communication and immune defence (Chiaramonte et al., 2014; Auguste et al., 2020; D'Alessio et al., 2021).

Among the protein signatures identified, some may be mainly, but not only, associated with the activation of programmed cell death. Deleted In Malignant Brain Tumors 1 (DMBT1) is a tumor growth suppressor and an effector of genetic resistance to hepatocarcinogenesis in rats and humans (Frau et al., 2012). Data obtained with the GBC-SD gallbladder cancer cell line demonstrated that its overexpression can down-regulate cell proliferation and induce apoptosis *via* stabilization of the phosphatase and tensin homolog (PTEN) and inhibition of the PI3K-Akt pathway, reducing xenograft tumor growth *in vivo* (Sheng et al., 2019). Similarly, expression of the huntingtin-interacting protein 1-related protein, a component of the clathrin-mediated endocytosis pathway, stimulated apoptosis and inhibited proliferation, locomotion and invasion of gastric tumor cells by acting on the Akt pathway (Zhu et al., 2020). The invertebrate semaphorin-1A is known to be similar to class-6 semaphorins of vertebrates (Battistini and Tamagnone, 2016), whose tumor-suppressing and apoptosis-stimulating roles have been recognized in different cancer cell models (Lu et al., 2012; Fard and Tamagnone, 2021). Peptides from the beta-1,3-glucan binding protein, a pattern recognition protein against invasive pathogens, of the pacific abalone *Haliotis discus hannai* showed pro-apoptotic properties against human cervical, lung and colon cancer cells (Nam et al., 2016). Up-regulation of the apoptosis-stimulating of p53 protein 1 in HepG2 cells exposed to the all-trans retinoic acid derivative 4-amino-2-trifluoromethyl-phenyl retinate was proven to result in cell cycle arrest and apoptosis (Liu et al., 2016). The zinc finger C3H1 domain-containing protein, which is known to modulate N6-methyladenosine RNA modification, has been considered a tumor suppressor correlated with a better survival rate in hepatocellular carcinoma (Huang et al., 2020). Conceivably, this might be based upon its interference with K-ras and ERK signaling as reported by Zhu et al. (2019) who observed the inhibition of proliferation and invasion of zinc finger C3H1 domain-containing protein over-expressing colorectal tumor cells. In breast cancer cell models, the up-regulation of galactosylceramide sulfotransferase, which increases the release of sulfatides from the sphingolipid, was found to be associated with the onset of programed cell death due to the decrease in the amount of the latter acting as an anti-apoptotic molecule (Suchanski et al., 2018). In the same models, the over-expression of ependymin-related protein 1, a poorly characterized transmembrane protein, was also shown to inhibit cell proliferation and migration leading to apoptosis *via* activation of the p53 signaling pathway (Liang et al., 2020). Ultimately, over-expression of *PRPF39*, coding for pre-mRNA-processing factor 39, in HepG2 cells appeared related to the acquisition of enhanced sensitivity to the cytotoxic action of cisplatin (Qin et al., 2021). This was ascribed, at least in part, to its acknowledged negative regulation on the expression of *TFDP2* coding for E2F dimerization partner 2 involved in the progression of the cell cycle, and positive regulation on the expression of *MAP3K4* coding for mitogen-activated protein kinase kinase kinase 4 which participates in apoptosis-promoting intracellular signaling (Stark et al., 2012).

In addition, other protein signatures may be mainly associated with the inhibition of cell migration, thus being related to the anti-metastatic property of the CFE preparation. In particular, the H3 chain of the inter-alpha trypsin inhibitor, an extracellular matrix component that binds to vitronectin, fibronectin and hyaluronic acid thereby influencing their biological activity (Lord et al., 2020), induces a significant decrease in the number of lung metastases in H460M cell-injected mice probably due to the increase in the cell adhesion rate (Paris et al., 2002). In addition, Sur-Erdem et al. (2020) reported that the giant actin-binding protein nesprin-1 is able to reverse

the tumorigenic phenotype of HuH7 hepatocellular carcinoma cells, whereas data from Huang et al. (2016) demonstrated that up-regulation of endoplasmic reticulum resident protein 44 determines the inhibition of human A549 lung cancer cell migration *via* an inositol 1,4,5-triphosphate receptor-dependent pathway. Notably, over-expression of the serum protein ficolin-2 was proven to significantly reduce the migratory and invasive behavior of liver cancer cells *in vitro* and *in vivo*, attenuating the epithelial-mesenchymal transition *via* stimulation of the TGFβ/Smad transduction pathway (Yang et al., 2016).

Finally, one of the identified protein signatures found may relate to the modulation of the autophagic flux. In fact, in retinal cells TBC1 domain family member 17, a RAB GTPase-activating protein, has been shown to impair autophagy, as well as the trafficking and recycling of transferrin receptors, both leading to the loss of cellular homeostasis and promotion of cell death (Chalasani et al., 2014).

Among the proteins listed, ficolin-2, semaphorin and putative endoplasmic reticulum resident protein 44 were reported to be contained in human and murine exosomes and released into body fluid (Looze et al., 2009; Biswas et al., 2019; Xia et al., 2021). Furthermore, our proteomic analysis of *H. tubulosa*'s CFE revealed the presence of histones H1 and H2B which can be considered additional markers of the nanovesicles (Auguste et al., 2020). In fact, extracellular histones are involved in exosome-mediated adhesion and could conceivably be involved in exosome uptake by target cells and the subsequent activation of signaling (Nangami et al., 2014; Muhsin-Shrafaldine et al., 2016; Ochieng et al., 2018).

In summary, we have shown that *H. tubulosa*'s CFE is cytotoxic towards hepatocellular carcinoma cells *in vitro*. A limitation of the present study is the lack of isolation and identification of the CFE component(s) to which the observed effects may be attributed. However, the proteomic profile analysis revealed a number of proteins that can seemingly play anti-cancer roles at different levels. Based on data from the literature (e.g. Khotimchenko, 2018) the contribution of varied sea cucumber-derived molecules, falling into the categories of triterpenes, glycosaminoglycans and cerebrosides, among others, cannot be excluded, as well as the existence of potential and complex synergic activities between these compounds. The data reported here strongly suggest that the water-soluble anti-HepG2 cell constituent(s) of the CFE is/are resistant to lyophilization, resuspension, and freeze-thawing cycles.

CONCLUSIONS

It is widely acknowledged that additives may be added to food directly or incorporated into the aliments in trace amounts during packaging, storage, or handling (Karunarathne et al., 2020). As reported by Vilela et al. (2018), packaging technologies are being developed to improve the safety and maintain the nutritional quality of minimally-processed food *via* the anti-microbial, anti-oxidant, and anticancer properties of the additives. Moreover, products from marine sources have great potential to be used as barrier coatings for multilayer packaging or edible coatings directly applied to food. In conclusion, considering these emerging technologies, the "active constituent(s)" present in the samples under study merit further investigation aimed at developing novel promising prevention and/or treatment agents and beneficial supplements for the formulation of functional food and food-packaging material.

Author contributions

Conceptualization, CL and MV; methodology, RB, LD, MM and VD; investigation, RB, GA, VL, LD and MM; data curation, CL; writing—original draft preparation, CL; writing—review and editing, CL and MV; supervision, CL, VA and MV; funding acquisition, VA. All authors have read and agreed to the published version of the manuscript.

Ethics approval

The "Assessorato regionale dell'agricoltura, sviluppo rurale e pesca mediterranea" of Sicily has approved the use of *Holothuria* in this study (authorization no. 87468 of 25.10.2021).

Conflict of interest

The authors declare no conflict of interest.

Acknowledgments

This work was supported by the University of Palermo (Italy) [grant Fondo Finalizzato alla Ricerca (FFR) 2021] to C.L. and M.V.

REFERENCES

Alper M, Güneş M. Evaluation of cytotoxic, apoptotic effects and phenolic compounds of sea cucumber *Holothuria tubulosa* (Gmelin, 1791) extracts. Turk J Vet Anim Sci. 2020;44:641-655.

Auguste M, Balbi T, Ciacci C, Canesi L. Conservation of cell communication systems in invertebrate host–defence mechanisms: possible role in immunity and disease. Biology. 2020;9:234.

Battistini C, Tamagnone L. Transmembrane semaphorins, forward and reverse signaling: have a look both ways. Cell Mol Life Sci. 2016;73:1609–22.

Baveja M, Sarkar A, Chakrabarty D. Hemotoxic and wound healing potential of coelomic fluid of sea-star *Astropecten indicus*. JoBAZ. 2018;79:27.

Biswas S, Mandal G, Roy Chowdhury S, Purohit S, Payne KK, Anadon C, et al. Exosomes produced by mesenchymal stem cells drive differentiation of myeloid cells into immunosuppressive M2-polarized macrophages in breast cancer. J Immunol. 2019;203:3447-60.

Boziaris IS. Food ingredients from the marine environment. Marine biotechnology meets food science and technology. Front Mar Sci. 2014;1:66.

Castelli G, Pelosi E, Testa U. Liver cancer: molecular characterization, clonal evolution and cancer stem cells. Cancers. 2017;9:127.

Chalasani ML, Kumari A, Radha V, Swarup G. E50K-OPTN-induced retinal cell death involves the Rab GTPase-activating protein, TBC1D17 mediated block in autophagy. PLoS One. 2014;9:e95758.

Chen X, Shen J, Xu J, Herald T, Smolensky D, Perumal R, et al. Sorghum phenolic compounds are associated with cell growth inhibition through cell cycle arrest and apoptosis in human hepatocarcinoma and colorectal adenocarcinoma cells. Foods. 2021;10:993.

Chiaramonte M, Russo D, Arizza V. Cell cooperation in Paracentrotus lividus (Lamarck, 1816): the role of the exosome in the cell-mediated cytotoxicity. In: Proceedings of the 75° National Congress of Italian Zoological Union, Bari, Italy, 22-25 September 2014. http://dx.doi.org/10.13140/2.1.1756.7687.

Chiaramonte M, Arizza V, La Rosa S, Queiroz V, Mauro M, Vazzana M, et al. Allograft inflammatory factor AIF-1: early immune response in the Mediterranean sea urchin Paracentrotus lividus. Zoology. 2020; 142:125815.

Correia-da-Silva M, Sousa E, Pinto MMM, Kijjoa A. Anticancer and cancer preventive compounds from edible marine organisms. Semin Cancer Biol. 2017;46: 55-64.

D'Alessio S, Buckley KM, Kraev I, Hayes P, Lange S. Extracellular vesicle signatures and post-translational protein deimination in purple sea urchin (*Strongylocentrotus purpuratus*) coelomic fluid—novel insights into echinodermata biology. Biology. 2021;10:866.

DiPaola RS. To arrest or not to G(2)-M Cell-cycle arrest: commentary re: A. K. Tyagi et al., Silibinin strongly synergizes human prostate carcinoma DU145 cells to doxorubicin-induced growth inhibition, G(2)-M arrest, and apoptosis. Clin Cancer Res. 2002;8: 3512-9; Clin Cancer Res. 2002;8:3311-4.

Donato MT, Tolosa L, Gómez-Lechón MJ. Culture and functional characterization of human hepatoma HepG2 cells. Methods Mol Biol. 2015;1250:77-93.

Fard D, Tamagnone L. Semaphorins in health and disease. Cytokine Growth Factor Rev. 2021;57:55-63.

Frau M, Simile MM, Tomasi ML, Demartis MI, Daino L, Seddaiu MA, et al. An expression signature of phenotypic resistance to hepatocellular carcinoma identified by cross-species gene expression analysis. Cell Oncol (Dordr). 2012;35:163-73.

Gao L, Loveless J, Shay C, Teng Y. Targeting ROS-mediated crosstalk between autophagy and apoptosis in cancer. Adv Exp Med Biol. 2020;1260:1-12.

Gibson SB. Investigating the role of reactive oxygen species in regulating autophagy. Meth Enzymol. 2013; 528:217-235.

Herencia F, Ubeda A, Ferrándiz ML, Terencio MC, Alcaraz MJ, García-Carrascosa M, et al. Anti-inflammatory activity in mice of extracts from Mediterranean marine invertebrates. Life Sci. 1998;62:PL115-20.

Huang X, Jin M, Chen YX, Wang J, Zhai K, Chang Y, et al. ERP44 inhibits human lung cancer cell migration mainly via IP3R2. Aging (Albany NY). 2016;8:1276-86.

Huang Y, Chen S, Qin W, Wang Y, Li L, Li Q, et al. A novel RNA binding protein-related prognostic signature for hepatocellular carcinoma. Front Oncol. 2020; 10:580513.

Inguglia L, Chiaramonte M, Di Stefano V, Schillaci D, Cammilleri G, Pantano L, et al. *Salmo Salar* fish waste oil: fatty acids composition and antibacterial activity. PeerJ. 2020;8:e9299.

Jiang J, Briedé JJ, Jennen DG, Van Summeren A, Saritas-Brauers K, Schaart G, et al. Increased mitochondrial ROS formation by acetaminophen in human hepatic cells is associated with gene expression changes suggesting disruption of the mitochondrial electron transport chain. Toxicol Lett. 2015;234:139-50.

Karunarathne S, Mendis E, Kim SK. The potential of developing additives from marine bioresources for the food industry. In: Encyclopedia of marine biotechnology, Vol. 5 (pp 3085-3107). Hoboken/NJ: Wiley, 2020.

Khotimchenko Y. Pharmacological potential of sea cucumbers. Int J Mol Sci. 2018;19:1342.

Kongara S, Karantza V. The interplay between autophagy and ROS in tumorigenesis. Front Oncol. 2012;2: 171.

Kumari R, Sahu MK, Tripathy A, Uthansingh K, Behera M. Hepatocellular carcinoma treatment: hurdles, advances and prospects. Hepat Oncol. 2018;5:HEP08.

Lazzara V, Arizza V, Luparello C, Mauro M, Vazzana M. Bright spots in the darkness of cancer: a review of starfishes-derived compounds and their anti-tumor action. Mar Drugs. 2019;17:617.

Liang X, Bai J, Chen B. Overexpression of EPDR1 has an antitumorigenic effect on breast cancer in vitro. Int J Clin Exp Pathol. 2020;13:2628-36.

Librizzi M, Longo A, Chiarelli R, Amin J, Spencer J, Luparello C. Cytotoxic effects of Jay Amin hydroxamic acid (JAHA), a ferrocene-based class I histone deacetylase inhibitor, on triple-negative MDA-MB231 breast cancer cells. Chem Res Toxicol. 2012;25:2608-16.

Liu H, Chen F, Zhang L, Zhou Q, Gui S, Wang Y. A novel all-trans retinoic acid derivative 4-amino-2-trifluoromethyl-phenyl retinate inhibits the proliferation of human hepatocellular carcinoma HepG2 cells by inducing G0/G1 cell cycle arrest and apoptosis via upregulation of p53 and ASPP1 and downregulation of iASPP. Oncol Rep. 2016;36:333-41.

Llovet JM, Kelley RK, Villanueva A, Singal AG, Pikarsky E, Roayaie S, et al. Hepatocellular carcinoma. Nat Rev Dis Primers. 2021;7:6.

Longo A, Librizzi M, Chuckowree IS, Baltus CB, Spencer J, Luparello C. Cytotoxicity of the urokinase-plasminogen activator inhibitor carbamimidothioic acid (4-boronophenyl) methyl ester hydrobromide (BC-11) on triple-negative MDA-MB231 breast cancer cells. Molecules. 2015;20:9879–89.

Looze C, Yui D, Leung L, Ingham M, Kaler M, Yao X, et al. Proteomic profiling of human plasma exosomes identifies PPARgamma as an exosome-associated protein. Biochem Biophys Res Commun. 2009;378:433-8.

Lord MS, Melrose J, Day AJ, Whitelock JM. The inter-α-trypsin inhibitor family: versatile molecules in biology and pathology. J Histochem Cytochem. 2020;68: 907-27.

Lu T, Tsai M, Hsiao C, Lai L, Chuang E. Expression and functions of semaphorins in cancer. Transl Cancer Res. 2012;1:74-87.

Luparello C. Marine animal-derived compounds and autophagy modulation in breast cancer cells. Foundations. 2021;1:3-20.

Luparello C, Ragona D, Asaro DML, Lazzara V, Affranchi F, Celi M, et al. Cytotoxic potential of the coelomic fluid extracted from the sea cucumber *Holothuria tubulosa* against triple-negative MDA-MB231 breast cancer cells. Biology. 2019a;8(4):76.

Luparello C, Asaro DML, Cruciata I, Hassell-Hart S, Sansook S, Spencer, J, et al. Cytotoxic activity of the histone deacetylase 3-selective inhibitor Pojamide on MDA-MB-231 triple-negative breast cancer cells. Int J Mol Sci. 2019b;20(4):804.

Luparello C, Mauro M, Lazzara V, Vazzana M. Collective locomotion of human cells, wound healing and their control by extracts and isolated compounds from marine invertebrates. Molecules. 2020a;25(11):2471.

Luparello C, Mauro M, Arizza V, Vazzana M. Histone deacetylase inhibitors from marine invertebrates. Biology. 2020b;9(12):429.

Luparello C, Ragona D, Asaro DML, Lazzara V, Affranchi F, Arizza, V, et al. Cell-free coelomic fluid extracts of the sea urchin *Arbacia lixula* impair mitochondrial potential and cell cycle distribution and stimulate reactive oxygen species production and autophagic activity in triple-negative MDA-MB231 breast cancer cells. J Mar Sci Eng. 2020c;8(4):261.

Ly JD, Grubb DR, Lawen A. The mitochondrial membrane potential (Δψm) in apoptosis; an update. Apoptosis. 2003;8:115–28.

Marchi S, Giorgi C, Suski JM, Agnoletto C, Bononi A, Bonora M, et al. Mitochondria-ROS crosstalk in the control of cell death and aging. J Signal Transduct. 2012;2012:329635.

Mauro M, Pérez-Arjona I, Perez EJB, Ceraulo M, Bou-Cabo M, Benson T, et al. The effect of low frequency noise on the behaviour of juvenile *Sparus aurata*. J Acoust Soc Am. 2020a;147:3795.

Mauro M, Lazzara V, Punginelli D, Arizza V, Vazzana M. Antitumoral compounds from vertebrate sister group: a review of mediterranean ascidians. Dev Comp Immunol. 2020b;108:103669.

Mauro M, Queiroz V, Arizza V, Campobello, D, Custódio MR, Chiaramonte M, et al. Humoral responses during wound healing in *Holothuria tubulosa* (Gmelin, 1788). Comp Biochem Physiol B Biochem Mol Biol. 2021;253:110550.

McGlynn KA, Petrick JL, El-Serag HB. Epidemiology of hepatocellular carcinoma. Hepatology. 2021;73 (Suppl 1):4-13.

Muhsin-Sharafaldine MR, Saunderson SC, Dunn AC, Faed JM, Kleffmann T, McLellan AD. Procoagulant and immunogenic properties of melanoma exosomes, microvesicles and apoptotic vesicles. Oncotarget. 2016;7:56279-94.

Murugan S, Amaravadi RK. Methods for studying autophagy within the tumor microenvironment. Adv Exp Med Biol. 2016;899:145-66.

Nam BH, Moon JY, Park EH, Kong HJ, Kim YO, Kim DG, et al. Antimicrobial and antitumor activities of novel peptides derived from the lipopolysaccharide- and β-1,3-glucan binding protein of the Pacific abalone *Haliotis discus hannai*. Mar Drugs. 2016;14:227.

Nangami G, Koumangoye R, Shawn Goodwin J, Sakwe AM, Marshall D, Higginbotham J, et al. Fetuin-A associates with histones intracellularly and shuttles them to exosomes to promote focal adhesion assembly resulting in rapid adhesion and spreading in breast carcinoma cells. Exp Cell Res. 2014;328:388-400.

Nelson MT, Short A, Cole, SL, Gross AC, Winter J, Eubank TD, et al. Preferential, enhanced breast cancer cell migration on biomimetic electrospun nanofiber 'cell highways'. BMC Cancer. 2014;14:825.

Ochieng J, Nangami G, Sakwe A, Rana T, Ingram S, Goodwin JS, et al. Extracellular histones are the ligands for the uptake of exosomes and hydroxyapatite-nanoparticles by tumor cells via syndecan-4. FEBS Lett. 2018;592:3274-85.

Paris S, Sesboüé R, Delpech B, Chauzy C, Thiberville L, Martin JP, et al. Inhibition of tumor growth and metastatic spreading by overexpression of inter-alpha-trypsin inhibitor family chains. Int J Cancer. 2002;97: 615-20.

Punginelli D, Schillaci D, Mauro M, Deidun A, Barone G, Arizza V, et al. The potential of antimicrobial peptides isolated from freshwater crayfish species in new drug development: a review. Dev Comp Immunol. 2021;126:104258.

Qin L, Zhan Z, Wei C, Li X, Zhang T, Li J. Hsa-circRNA-G004213 promotes cisplatin sensitivity by regulating miR-513b-5p/PRPF39 in liver cancer. Mol Med Rep. 2021;23:421.

Schillaci D, Cusimano MG, Cunsolo V, Saletti R, Russo D, Vazzana M, et al. Immune mediators of sea-cucumber *Holothuria tubulosa* (Echinodermata) as source of novel antimicrobial and anti-staphylococcal biofilm agents. AMB Express. 2013;3:35.

Senthilkumar K, Kim SK. Marine invertebrate natural products for anti-inflammatory and chronic diseases. Evid Based Complement Alternat Med. 2013;2013: 572859.

Sheng S, Jiwen W, Dexiang Z, Bohao Z, Yueqi W, Han L, et al. DMBT1 suppresses progression of gallbladder carcinoma through PI3K/AKT signaling pathway by targeting PTEN. Biosci Biotechnol Biochem. 2019;83: 2257-64.

Stark AL, Delaney SM, Wheeler HE, Im HK, Dolan ME. Functional consequences of PRPF39 on distant genes and cisplatin sensitivity. Hum Mol Genet. 2012; 21:4348-55.

Suarez-Arnedo A, Torres Figueroa F, Clavijo C, Arbeláez P, Cruz JC, Muñoz-Camargo C. An image J plugin for the high throughput image analysis of in vitro scratch wound healing assays. PLoS One. 2020;15: e0232565.

Suchanski J, Grzegrzolka J, Owczarek T, Pasikowski P, Piotrowska A, Kocbach B, et al. Sulfatide decreases the resistance to stress-induced apoptosis and increases P-selectin-mediated adhesion: a two-edged sword in breast cancer progression. Breast Cancer Res. 2018; 20(1):133.

Suleria HA, Osborne S, Masci P, Gobe G. Marine-based nutraceuticals: an innovative trend in the food and supplement industries. Mar Drugs. 2015;13:6336-51.

Sun Y, Zou H, Yang L, Zhou M, Shi X, Yang Y, et al. Effect on the liver cancer cell invasion ability by studying the associations between autophagy and TRAP1 expression. Oncol Lett. 2018;16:991-7.

Sur-Erdem I, Hussain MS, Asif M, Pınarbası N, Aksu AC, Noegel AA. Nesprin-1 impact on tumorigenic cell phenotypes. Mol Biol Rep. 2020;47:921-34.

Suresh D, Srinivas AN, Kumar DP. Etiology of hepatocellular carcinoma: special focus on fatty liver disease. Front Oncol. 2020;10:601710.

Tawfik MM, Eissa N, Althobaiti F, Fayad E, Abu Almaaty AH. Nomad jellyfish *Rhopilema nomadica* venom induces apoptotic cell death and cell cycle arrest in human hepatocellular carcinoma HepG2 cells. Molecules. 2021;26:5185.

Vazzana M, Mauro M, Ceraulo M, Dioguardi M, Papale E, Mazzola S, et al. Underwater high frequency noise: biological responses in sea urchin *Arbacia lixula* (Linnaeus, 1758). Comp Biochem Physiol Part A Mol Integr Physiol. 2020a;242:110650.

Vazzana M, Ceraulo M, Mauro M, Papale E, Dioguardi M, Mazzola S, et al. Effects of acoustic stimulation on biochemical parameters in the digestive gland of mediterranean mussel *Mytilus galloprovincialis* (Lamarck, 1819). J Acoust Soc Am. 2020b;147:2414–22.

Vilela C, Kurek M, Hayouka Z, Röcker B, Yildirim S, Antunes MDC, et al. A concise guide to active agents for active food packaging. Trends Food Sci Technol. 2018;80:212-22.

Xia T, Tian H, Zhang K, Zhang S, Chen W, Shi S, et al. Exosomal ERp44 derived from ER-stressed cells strengthens cisplatin resistance of nasopharyngeal carcinoma. BMC Cancer. 2021;21:1003.

Yang G, Liang Y, Zheng T, Song R, Wang J, Shi H, et al. FCN2 inhibits epithelial-mesenchymal transition-induced metastasis of hepatocellular carcinoma via TGF-β/Smad signaling. Cancer Lett. 2016;378:80-6.

Zhang J, Wang X, Vikash V, Ye Q, Wu D, Liu Y, et al. ROS and ROS-mediated cellular signaling. Oxid Med Cell Longev. 2016;2016:4350965.

Zheng LH, Wang YJ, Sheng J, Wang F, Zheng Y, Lin XK, et al. Antitumor peptides from marine organisms. Mar Drugs. 2011;9:1840–59.

Zhu C, Zhao M, Fan L, Cao X, Xia Q, Zhou J, et al. Chitopentaose inhibits hepatocellular carcinoma by inducing mitochondrial mediated apoptosis and suppressing protective autophagy. Bioresour Bioprocess. 2021b;8:4.

Zhu D, Zhou J, Zhao J, Jiang G, Zhang X, Zhang Y, et al. ZC3H13 suppresses colorectal cancer proliferation and invasion via inactivating Ras-ERK signaling. J Cell Physiol. 2019;234:8899-907.

Zhu J, Wang X, Guan H, Xiao Q, Wu Z, Shi J, et al. HIP1R acts as a tumor suppressor in gastric cancer by promoting cancer cell apoptosis and inhibiting migration and invasion through modulating Akt. J Clin Lab Anal. 2020;34(9):e23425.

Zhu Y, Tian Y, Wang N, Chang Y, Xue C, Wang J. Structure-function relationship analysis of fucoidan from sea cucumber (*Holothuria tubulosa*) on ameliorating metabolic inflammation. J Food Biochem. 2021a;45:e13500.

Zmemlia N, Bejaoui S, Khemiri I, Bouriga N, Louiz I, El-Bok S, et al. Biochemical composition and antioxidant potential of the edible Mediterranean sea cucumber *Holothuria tubulosa*. Grasas y Aceites. 2020;71: e364.